INNOV 2024

The Thirteenth International Conference on Communications, Computation, Networks and Technologies

ISBN: 978-1-68558-196-1

September 29 - October 03, 2024

Venice, Italy

INNOV 2024 Editors

Hans-Werner Sehring, NORDAKADEMIE gAG, Germany

Eugen Borcoci, National University of Science and Technology POLITEHNICA Bucharest, Romania

INNOV 2024

Forward

The Thirteenth International Conference on Communications, Computation, Networks and Technologies (INNOV 2024), held on September 29 – October 3, 2024 in Venice, Italy, aimed at addressing recent research results and forecasting challenges on selected topics related to communications, computation, networks and technologies.

Considering the importance of innovative topics in today's technology-driven society, there is a paradigm shift in classical-by-now approaches, such as networking, communications, resource sharing, collaboration and telecommunications. Recent achievements demand rethinking available technologies and considering the emerging ones.

The conference had the following tracks:

☐ Communications
☐ Networking
☐Computing
☐Web Semantic and Data Processing
☐Security, Trust, and Privacy

We take here the opportunity to warmly thank all the members of the INNOV 2024 technical program committee, as well as the numerous reviewers. The creation of such a high quality conference program would not have been possible without their involvement. We also kindly thank all the authors that dedicated much of their time and effort to contribute to INNOV 2024. We truly believe that, thanks to all these efforts, the final conference program consisted of top quality contributions.

Also, this event could not have been a reality without the support of many individuals, organizations and sponsors. We also gratefully thank the members of the INNOV 2024 organizing committee for their help in handling the logistics and for their work that made this professional meeting a success.

We hope that INNOV 2024 was a successful international forum for the exchange of ideas and results between academia and industry and to promote further progress in the areas of communication, computation, networks and technologies. We also hope that Venice provided a pleasant environment during the conference and everyone saved some time for exploring this beautiful city

INNOV 2024 Steering Committee

Sean Sturley, University of the West of Scotland, UK
Yeim-Kuan Chang, National Cheng Kung University, Taiwan

INNOV 2024 Publicity Chair

Lorena Parra Boronat, Universitat Politecnica de Valencia, Spain
Sandra Viciano Tudela, Universitat Politecnica de Valencia, Spain
Jose Miguel Jimenez, Universitat Politecnica de Valencia, Spain

Francisco Javier Díaz Blasco, Universitat Politecnica de Valencia, Spain
Ali Ahmad, Universitat Politecnica de Valencia, Spain

INNOV 2024

Committee

INNOV 2024 Steering Committee

Sean Sturley, University of the West of Scotland, UK
Yeim-Kuan Chang, National Cheng Kung University, Taiwan

INNOV 2024 Publicity Chair

Lorena Parra Boronat, Universitat Politecnica de Valencia, Spain
Sandra Viciano Tudela, Universitat Politecnica de Valencia, Spain
Jose Miguel Jimenez, Universitat Politecnica de Valencia, Spain
Francisco Javier Díaz Blasco, Universitat Politecnica de Valencia, Spain
Ali Ahmad, Universitat Politecnica de Valencia, Spain

INNOV 2024 Technical Program Committee

Lavanya Addepalli, Universitat Politecnica de Valencia, Spain
Akshit Aggarwal, Indian Institute of Information Technology Guwahati, India
Amjad Ali,University of Swat, Pakistan
Eugen Borcoci, National University of Science and Technology POLITEHNICA Bucharest, Romania
Constantin F. Caruntu, Gheorghe Asachi Technical University of Iasi, Romania
YK Chang, National Cheng Kung University, Taiwan
DeJiu Chen, KTH Royal Institute of Technology, Sweden
Albert M. K. Cheng, University of Houston, USA
Karl Cox, University of Brighton, UK
Daniela D'Auria, Free University of Bozen-Bolzano, Italy
Panagiotis Fouliras, University of Macedonia, Thessaloniki, Greece
Marco Furini, University of Modena and Reggio Emilia, Italy
Laura García, Universitàt Politècnica de València, Spain
Nikolaos Gorgolis, University of Patras, Greece
Victor Govindaswamy, Concordia University Chicago, USA
Jens Grambau, HdM Stuttgart, Germany
Qiang He, Swinburne University of Technology, Australia
Mehdi Hosseinzadeh, Washington University in St. Louis, USA
Shih-Chang Huang, National Formosa University, Taiwan
Wen-Jyi Hwang, National Taiwan Normal University, Taipei, Taiwan
Sergio Ilarri, University of Zaragoza, Spain
AKM Kamrul Islam, North Carolina A&T State University, USA
Brigitte Jaumard, Concordia University, Canada
Alexey Kashevnik, SPIIRAS, Russia
Sameh Kchaou, University of Sfax, Tunisia
Khaled Khankan, Taibah University, Saudi Arabia

Copyright Information

For your reference, this is the text governing the copyright release for material published by IARIA.

The copyright release is a transfer of publication rights, which allows IARIA and its partners to drive the dissemination of the published material. This allows IARIA to give articles increased visibility via distribution, inclusion in libraries, and arrangements for submission to indexes.

I, the undersigned, declare that the article is original, and that I represent the authors of this article in the copyright release matters. If this work has been done as work-for-hire, I have obtained all necessary clearances to execute a copyright release. I hereby irrevocably transfer exclusive copyright for this material to IARIA. I give IARIA permission or reproduce the work in any media format such as, but not limited to, print, digital, or electronic. I give IARIA permission to distribute the materials without restriction to any institutions or individuals. I give IARIA permission to submit the work for inclusion in article repositories as IARIA sees fit.

I, the undersigned, declare that to the best of my knowledge, the article is does not contain libelous or otherwise unlawful contents or invading the right of privacy or infringing on a proprietary right.

Following the copyright release, any circulated version of the article must bear the copyright notice and any header and footer information that IARIA applies to the published article.

IARIA grants royalty-free permission to the authors to disseminate the work, under the above provisions, for any academic, commercial, or industrial use. IARIA grants royalty-free permission to any individuals or institutions to make the article available electronically, online, or in print.

IARIA acknowledges that rights to any algorithm, process, procedure, apparatus, or articles of manufacture remain with the authors and their employers.

I, the undersigned, understand that IARIA will not be liable, in contract, tort (including, without limitation, negligence), pre-contract or other representations (other than fraudulent misrepresentations) or otherwise in connection with the publication of my work.

Exception to the above is made for work-for-hire performed while employed by the government. In that case, copyright to the material remains with the said government. The rightful owners (authors and government entity) grant unlimited and unrestricted permission to IARIA, IARIA's contractors, and IARIA's partners to further distribute the work.

Table of Contents

Reconfigurable Intelligent Surface Assisted MIMO SWIPT System

Hsuan-Fu Wang
Department of Aeronautical Engineering
National Formosa University
Yunlin, Taiwan

Fang-Biau Ueng
Department of Electrical Engineering
National Chung Hsing University
Taichung, Taiwan

Huang-Wei Shen
Department of Electrical Engineering
National Chung Hsing University
Taichung, Taiwan

***Abstract*—The large-scale Internet of Things (IoTs) of B5G networks must face the arduous challenge of bandwidth limitations. Although millimeter wave (mmWave) technology can provide greater bandwidth at the cost of complex processors in harsh environments, it can be a possible solution for building large-scale IoTs, but its cost and power requirements become obstacles to widespread adoption. In this context, Re-configurable Intelligent Surfaces (RISs) can be a key technology to meet this challenge. In this paper, we study the B5G RIS-assisted MIMO simultaneous wireless-information and power-transfer (SWIPT) mmWave large-scale IoTs, where active BS transmitted beamformer and passive RIS reflection vector are jointly optimized to maximize the minimum signal-to-interference-plus-noise-ratio (SINR) of all the information decoders (ID) and at the same time, the minimum harvested power of all the energy receivers (ER) is maintained. Some simulation examples are given to demonstrate the effectiveness of the proposed system.**

Keywords—mmWave, RIS, SWIPT

I. INTRODUCTION

Massive MIMO uses a large number of antennas to obtain large beamforming gains. In fact, under similar conditions, both massive MIMO and RIS techniques can produce similar signal-to-noise ratio (SNR) gains. However, RIS passively achieves this beamforming gain. In this paper, active beamforming through the transmitter antenna array and passive beamforming through the RIS in the channel can compensate each other and provide greater gain when both are optimized together, which is exactly what goals of this paper. Although massive MIMO technology can significantly improve the efficiency of wireless information transfer (WIT) and wireless power transfer (WPT) in emerging IoT networks by exploiting the gain of large arrays, this usually comes at a high cost [1]-[3]. As a remedy, in so-called hybrid implementations, a much smaller number of radio frequency (RF) chains than transmit/receive antennas can be used, which can also result in high hardware costs, high signal processing overhead, and high energy consumption, hindering actual implementation. As a cost-effective alternative to massive MIMO technology, RIS enables unprecedented spectral and energy efficiency, especially in complex propagation scenarios that suffer from severe signal blocking. However, because RIS is essentially a reconfigurable metal surface with a large number of passive reflective elements, it cannot perform as complex signal processing as large arrays and active MIMO repeaters, and is usually performed with lower hardware cost and low power consumption. By adjusting the phase shift and amplitude attenuation of each RIS reflective element, a good wireless propagation environment can be actively constructed for WIT and WPT [4][5]. In view of the above advantages, research on RIS-assisted communication for various wireless systems such as MISO systems [6][7], point-to-point MIMO systems [8], multi-cell multi-user MIMO systems [9], and MIMO-OFDM systems [10] [11] attracted attention. These studies usually assume perfect channel state information (CSI). In fact, traditional training-based channel estimation schemes cannot be directly applied due to the lack of fundamental frequency processing capability of RIS operating without RF chains and the need to estimate a large number of RIS-related channels. As an alternative, under the assumption of uplink-downlink channel reciprocity, for flat frequency channels and frequency selective channels, various channel estimation schemes using RIS grouping strategies have been proposed previously [10]-[13].

Nonetheless, there are new challenges to integrate RF energy harvesting and advanced WIT technologies for sustainable green IoT networks. To this end, Simultaneous Wireless Information and Power Transfer (SWIPT) has been evaluated as an attractive innovative technology [13]. Recently, there has been increasing interest in RIS-based SWIPT systems [9]. For example, [13] studied weighted harvested energy maximization in a RIS-assisted MISO SWIPT system and demonstrated that dedicated energy beamforming is practically not required. As a further development, the maximization of the minimum harvested energy among all energy receivers (ERs) in this system is studied from a fairness perspective. By deploying multiple RIS, [13] further investigated total transmit power minimization subject to separate QoS constraints at the Information Decoder (ID) and ER. [9] considered a more general RIS-assisted MIMO SWIPT system and studied the weighted sum rate maximization of all IDs while guaranteeing a certain minimum total harvested energy across all ERs. Various advanced communication technologies in IoT networks, such as NOMA, Physical Layer Security, and Mobile Edge Computing (MEC), have also been integrated with this technology together. RIS achieves better system performance, so in this paper, we consider a RIS-assisted MIMO SWIPT system consisting of a multi-antenna base station (BS), a RIS to assist communication, and multiple SWIPT-enabled systems. It consists of several IoT devices, and RIS is deployed to assist SWIPT from the BS to these IoT devices. From a fairness perspective, we further investigate the maximization of the minimum SINR among all IDs by jointly optimizing the active BS transmit beamforming vector and the passive RIS reflection coefficient, premised on the minimum total harvested energy required for all ERs.

II. SYSTEM MODEL AND PROBLEM FORMULATION

This section introduces the system model and problem description. We first introduce the architecture of the entire system, and then describe our goals and the problems. We consider an RIS-assisted wireless communication system, in which the RIS is deployed to assist the multi-antenna APs in

the SWIPT system. It is transmitted from the AP of M antennas to two parts, including information user (IU) and energy user (EU), the number of IU is K_I, and the number of EU is K_ε. For simplicity, we consider linear transmit precoding at the AP and assume that each IU/EU is assigned a separate information/energy beam, without loss of generality. Therefore, the transmission signal from the AP can be expressed as

$$x = \sum_{i\epsilon K_I} w_i s_i^I + \sum_{\mathrm{j}\in K_\varepsilon} v_j s_j^E \tag{1}$$

And $w_i \in C^{M\times 1}$ is the precoding vector of IU, $v_j \in C^{M\times 1}$ is the precoding vector of EU, s_i^I represents the message bearing signal, and s_j^E represents the energy signal. s_i^I are assumed to be independent and identically distributed signal with zero mean and variance one, while s_j^E carry no information, they can be any random signals. Therefore, the total transmit power required by the AP is expressed as

$$E(x^H x) = \sum_{i\epsilon K_I} \|w_i\|^2 + \sum_{\mathrm{j}\in K_\varepsilon} \|v_j\|^2 \tag{2}$$

Next is the part of the signal received by the IU, $h_{\mathrm{d},k}^H \in C^{1\times M}$ is the channel directly transmitted by the AP to the IU, $h_{\mathrm{g},k}^H \in C^{1\times L}$ is the channel that the RIS transmits to the IU, $e_{\mathrm{d},k}^H$ is the channel that the AP transmits directly to the EU, $e_{\mathrm{g},k}^H$ is the channel that the RIS transmits to the EU, $W_g(l)$ indicates the channel transmitted from the AP to the RIS, and $\Phi_g^H(l)$ represents the reflective element channel in the RIS. Since implementing independent control of reflection amplitude and phase is expensive in reality, for simplicity, it is actually advantageous to design each element to maximize signal reflections. Therefore, we express the signal received by the IU from AP to IU and AP to RIS and then to IU as the following equations:

$$y_k^I = (\sum_{l=1}^{L} h_{g,k}^H(l)\Phi_g^H(l)W_g(l) + h_{\mathrm{d},k}^H)x + \sigma_k \tag{3}$$

Here $\sigma_k \sim CN(0,\sigma_k^2)$ is an independent and identically distributed Gaussian noise, and we simplify equation (3) and rewrite it as (4):

$$y_k^I = (h_{g,k}^H \Phi_g^H W_g + h_{\mathrm{d},k}^H)x + \sigma_k \tag{4}$$

where $h_{g,k}^H \in C^{N\times N}$, $W_g \in C^{N\times M}$ and $\Phi_g^H \in C^{N\times N}$ are represented by equations (5) and (6), respectively,

$$h_{g,k}^H = \begin{bmatrix} h_{g,k}^H(1) \\ \dots \\ h_{g,k}^H(L) \end{bmatrix}, W_g = \begin{bmatrix} W_g(1) \\ \dots \\ W_g(L) \end{bmatrix} \tag{5}$$

$$\Phi_g^H = \begin{bmatrix} \Phi_g^H(1) & 0 & 0 \\ 0 & \dots & 0 \\ 0 & 0 & \Phi_g^H(L) \end{bmatrix} \tag{6}$$

Since the energy beam carries no information but a pseudo-random signal, its waveform can be assumed to be known at the AP and each IU prior to data transmission. We hypothesize that the interference they cause can be canceled at each IU, which contributes to the fundamental performance limitations of our SWIPT system and the study of the impact of RIS on energy beamforming. Therefore, we express SINR by Equation (7):

$$\mathrm{SINR}_k = \gamma_k = \frac{\left|\sum_{\mathrm{g}=1}^{G} h_{g,k}^H \Phi_g^H W_g w_i\right|^2}{\sum_{k=1,k\neq i}^{K} \left|\sum_{\mathrm{g}=1}^{G} h_{g,k}^H \Phi_g^H W_g w_k\right|^2 + \sigma_i^2} \tag{7}$$

On the other hand, it is the part of the energy received by the EU. We express the energy received by the EU with Equation (8):

$$Q_j = \sum_{i\epsilon K_i} \left|(e_{g,j}^H \Phi_g^H W_g + e_{\mathrm{d},j}^H)w_i\right|^2 + \sum_{i\epsilon K_\varepsilon} \left|(e_{g,j}^H \Phi_g^H W_g + e_{\mathrm{d},j}^H)v_m\right|^2 \tag{8}$$

Then comes the problem description part, our goal is to maximize the transmission rate of the entire system through optimization subject to the constraints of the transmission power and the energy harvesting at the EU, we formulate the problem description as Eq. (9):

$$\underset{P,\Phi_g}{\text{maximize}}\ f_1(P,\Phi_g) = \sum_{k=1}^{K} z_k \log_2(1+\gamma_k) \tag{9}$$

$$\text{subject to } \sum_{i\epsilon K_I} \|w_i\|^2 + \sum_{\mathrm{j}\in K_\varepsilon} \|v_j\|^2 \le P, \tag{10}$$

$$\sum_{i\epsilon K_i} \left|(e_{g,j}^H \Phi_g^H W_g + e_{\mathrm{d},j}^H)w_i\right|^2 + \sum_{i\epsilon K_\varepsilon} \left|(e_{g,j}^H \Phi_g^H W_g + e_{\mathrm{d},j}^H)v_m\right|^2 \ge E_j \tag{11}$$

$$0 < \theta_n \le 2\pi, \forall n \in N. \tag{12}$$

Where z_k is the data weight assigned to the kth IU, P represents the maximum transmission power, $E_j > 0$ is the least energy received by each energy user, and θ_n represents the phase of the RIS.

III. The Proposed Methods and Algorithm

First, we change the formula of power limit into the form of rank, such as (13):

$$\begin{aligned} &\underset{P,\Phi_g}{\text{maximize}}\ f_1(P,\Phi_g) = \sum_{k=1}^{K} z_k\, log_2(1+\gamma_k) \\ &\text{subject to } \sum_{k\in K} Tr(W_k) + Tr(V_l) \le P, \\ &\sum_{i\epsilon K_i} \left|(e_{g,j}^H \Phi_g^H W_g + e_{\mathrm{d},j}^H)w_i\right|^2 + \\ &\sum_{i\epsilon K_\varepsilon} \left|(e_{g,j}^H \Phi_g^H W_g + e_{\mathrm{d},j}^H)v_m\right|^2 \ge E_j, \\ &0 < \theta_n \le 2\pi, \forall n \in N. \end{aligned} \tag{13}$$

Next, we use the Lagrangian dual transformation [3] that the term $\sum_{k=1}^{K} z_k\, log_2(1+\gamma_k)$ can be converted into $\sum_{k=1}^{K} z_k\, ln(1+\alpha_k) - z_k\alpha_k + \frac{z_k(1+\alpha_k)\gamma_k}{1+\gamma_k}$. Therefore, we transform f_1 into problem f_2, which is represented by equation (14):

$$\underset{P,\Phi_g,\alpha}{\text{maximize}}\ f_2(P,\Phi_g,\alpha) = \sum_{k=1}^{K} z_k\, ln(1+\alpha_k) - z_k\alpha_k + \frac{z_k(1+\alpha_k)\gamma_k}{1+\gamma_k} \tag{14}$$

$$\text{subject to} \quad tr(PP^H) \le P, \tag{15}$$

$$\sum_{i\epsilon K_i}\left|e_j^H w_i\right|^2+\sum_{i\epsilon K_\varepsilon}\left|e_j^H v_m\right|^2\geq E_j, \quad (16)$$

$$\theta_{g,m}\in F_c\,,\forall g,\forall m. \quad (17)$$

f_1 and f_2 are equivalent, so solving f_1 is equivalent to solving f_2, where $\alpha=[\alpha_1,\cdots,\alpha_k]^T$ is the additional vector generated after conversion. In addition, the formula of the transmission power is simplified again, and the mathematical symbol e_j^H is used to represent $e_j^H=e_{g,j}^H\Phi_g^H W_g+e_{\mathrm{d},j}^H$. After the conversion, we give α_k, optimize P and Φ_g, and rewrite the problem f_2 into the problem f_3 as follows,

$$\underset{P,\Phi_g}{\text{maximize}}\, f_3\left(P,\Phi_g\right)=\sum_{k=1}^{K}\frac{z_k(1+\alpha_k)\gamma_k}{1+\gamma_k} \quad (18)$$

$$\text{subject to (15), (16), (17).}$$

Given the set $\{\Phi_1,\cdots,\Phi_g\}$, for convenience, we use the mathematical notation $\tilde{h}_k^H$ to represent (19):

$$\tilde{h}_k^H=\sum_{\mathrm{g}=1}^{G}h_{g,k}^H\Phi_g^H W_g \quad (19)$$

Substitute formula (19) into the above SINR formula, that is, formula (7), and rearrange f_3 to generate f_4, such as formula (20):

$$\underset{P}{\text{maximize}}\, f_4\,(P)=\sum_{k=1}^{K}\frac{\bar{\alpha}_k\left|\tilde{h}_k^H p_k\right|^2}{\sum_{j=1}^{K}\left|\tilde{h}_k^H p_j\right|^2+\sigma_u^2} \quad (20)$$

$$\text{subject to (15).}$$

where the symbol $\bar{\alpha}_k=z_k(1+\alpha_k)$, and we can see that f_4 is a multi-score programming problem, so we can use Quadratic Transform (QT) [3][4] to convert f_4 to f_5, such as formula (21):

$$\underset{P,\beta}{\text{maximize}}\, f_5\,(P,\beta\,)=\sum_{k=1}^{K}2\sqrt{\bar{\alpha}_k}\mathfrak{R}\{\beta_k^*\tilde{h}_k^H p_k\}-|\beta_k|^2\Big(\sum_{\mathrm{j}=1}^{K}\left|\tilde{h}_k^H p_j\right|^2+\sigma_u^2\Big) \quad (21)$$

And $\beta=[\beta_1,\cdots,\beta_k]^T$ is the additional vector generated after the QT conversion. Using $\frac{\partial f_5}{\partial\beta_k}=0$, such as equations (22) and (23), and given P, the optimal solution of β_k can be described as follows:

$$\frac{\partial f_5}{\partial\beta_k}=2\sqrt{\bar{\alpha}_k}\tilde{h}_k^H p_k-2\beta_k\left(\sum_{\mathrm{j}=1}^{K}\left|\tilde{h}_k^H p_j\right|^2+\sigma_u^2\right)=0 \quad (22)$$

$$\beta_k\left(\sum_{\mathrm{j}=1}^{K}\left|\tilde{h}_k^H p_j\right|^2+\sigma_u^2\right)=\sqrt{\bar{\alpha}_k}\tilde{h}_k^H p_k \quad (23)$$

$$\hat{\beta}_k=\frac{\sqrt{\bar{\alpha}_k}\tilde{h}_k^H p_k}{\sum_{j=1}^{K}\left|\tilde{h}_k^H p_j\right|^2+\sigma_u^2} \quad (24)$$

Since the problem f_5 is a convex problem about p_{k}, using the Lagrange multiplier method, given β, the optimal solution of p_k can be described as equation (25):

$$\hat{p}_k=\sqrt{\bar{\alpha}_k}\,\beta_k\left(\mu I_N+\sum_{i=1}^{k}|\beta_i|^2\tilde{h}_i\,\tilde{h}_i^H\right)^{-1}\tilde{h}_k \quad (25)$$

Next, we simplify the mathematical formula to facilitate the operation and derivation, $\tilde{h}_k^H p_j$ can be expressed as formula (26):

$$\tilde{h}_k^H p_j=\sum_{g=1}^{G}\theta_g^H\,\mathrm{diag}(h_{g,k}^H)W_g p_j \quad (26)$$

Where $\boldsymbol{\theta}_g$ is defined as $\boldsymbol{\theta}_g=\left[\theta_{g,1},\cdots,\theta_{g,M}\right]^T$ and $v_{g,k,j}$ is defined as $v_{g,k,j}=\mathrm{diag}(h_{g,k}^H)W_g p_j$. Given α and P, we rewrite the problem f_4 into the problem f_6, as shown in equation (27):

$$\underset{\theta_g}{\text{maximize}}\, f_6\left(\theta_g\right)=\sum_{k=1}^{K}\frac{\bar{\alpha}_k\left|\sum_{g=1}^{G}\theta_g^H v_{g,k,k}\right|^2}{\sum_{j=1}^{K}\left|\sum_{g=1}^{G}\theta_g^H v_{g,k,j}\right|^2+\sigma_u^2} \quad (27)$$

$$\text{subject to}\ \left|\theta_{g,m}\right|^2=1,\ \forall g,\ \forall m.$$

In order to facilitate the subsequent derivation, we first construct several symbols to represent the following equations, as shown in equations (28) and (29):

$$\boldsymbol{\Theta}=[\theta_1,\theta_2,\cdots,\theta_G] \quad (28)$$

$$V_{k,j}=\left[v_{1,\mathrm{k},j},v_{2,k,j},\cdots,v_{G,k,j}\right] \quad (29)$$

After the construction is completed, we can rewrite the problem f_6 into the problem f_7, as shown in equation (30):

$$\underset{\tilde{\theta}}{\text{maximize}}\, f_7\left(\tilde{\theta}\right)=\sum_{k=1}^{K}\frac{\bar{\alpha}_k\left|tr\left(\Theta^H V_{k,k}\right)\right|^2}{\sum_{j=1}^{K}\left|tr\left(\Theta^H V_{k,j}\right)\right|^2+\sigma_u^2} \quad (30)$$

$$=\sum_{k=1}^{K}\frac{\bar{\alpha}_k\left|\tilde{\theta}^H\,\tilde{v}_{k,k}\right|^2}{\sum_{j=1}^{K}\left|\tilde{\theta}^H\,\tilde{v}_{k,j}\right|^2+\sigma_u^2} \quad (31)$$

$$\text{subject to}\ \left|\theta_{g,m}\right|^2=1,\ \forall g,\ \forall m.$$

where $\tilde{\theta}$ is expressed as $\tilde{\theta}=\mathrm{vec}(\Theta)$, and $\tilde{v}_{k,j}$ is expressed as $\tilde{v}_{k,j}=\mathrm{vec}(V_{k,j})$. Next, we transform problem f_7 into problem f_8 using quadratic transformation (QT) [3], as shown in Eq. (32):

$$\underset{\tilde{\theta}\,,\rho}{\text{maximize}}\, f_8\left(\tilde{\theta}\,,\rho\right)=\sum_{k=1}^{K}2\sqrt{\bar{\alpha}_k}\mathfrak{R}\{\rho_k^*\tilde{\theta}^H\,\tilde{v}_{k,k}\}-|\rho_k|^2\Big(\sum_{\mathrm{j}=1}^{K}\left|\tilde{\theta}^H\,\tilde{v}_{k,j}\right|^2+\sigma_u^2\Big) \quad (32)$$

$$\text{subject to}\ \left|\theta_{g,m}\right|^2=1,\ \forall g,\ \forall m.$$

After conversion, $\rho=[\rho_1,\cdots,\rho_k]^T$ is the additional vector generated by the secondary conversion. Using the Lagrange multiplier method [3], the optimal solution of ρ_k is shown in formula (33):

$$2\sqrt{\bar{\alpha}_k}\tilde{\theta}^H\,\tilde{v}_{k,k}-2\rho_k\left(\sum_{\mathrm{j}=1}^{K}\left|\tilde{\theta}^H\,\tilde{v}_{k,j}\right|^2+\sigma_u^2\right)=0 \quad (33)$$

$$\rho_k\left(\sum_{\mathrm{j}=1}^{K}\left|\tilde{\theta}^H\,\tilde{v}_{k,j}\right|^2+\sigma_u^2\right)=\sqrt{\bar{\alpha}_k}\tilde{\theta}^H\,\tilde{v}_{k,k} \quad (34)$$

$$\hat{\rho}_k=\frac{\sqrt{\bar{\alpha}_k}\tilde{\theta}^H\tilde{v}_{k,k}}{\sum_{j=1}^{K}\left|\tilde{\theta}^H\tilde{v}_{k,j}\right|^2+\sigma_u^2} \quad (35)$$

IV. Simulation Results

In this section, we use MATLAB software to perform simulations to compare the performance of the entire SWIPT system with and without RIS. The simulation parameters include: the number of users (K), the number of antennas (N), the number of reflective elements (M), and the transmission power (P). For the channel part, we use the Rayleigh channel. Figure 1 is the schematic diagram of the simulation environment.

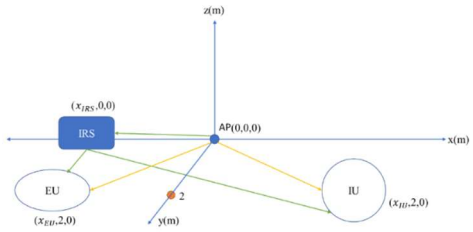

Fig. 1. Simulation Schematic

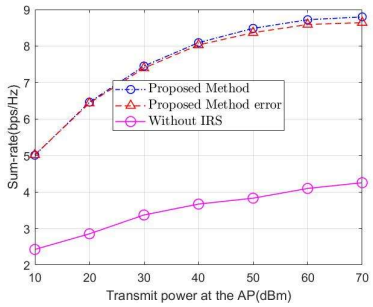

Fig. 2. Comparison of transmission sum rates when the number of users (information receiving end and energy receiving end) is 2, the number of antennas is 16, and the number of reflective elements is 20.

Figure 2 shows the performance comparisons employing 2 users (information receiving end and energy receiving end), 16 antennas and 20 reflective elements with and without RIS. The error part is the 10% parameter error of our proposed method. In addition, whether it is a system with RIS or a system without RIS, the two transmission powers are fixed. It can be seen from the figure that with RIS, the total rate is faster than that without RIS, from 10-dBm faster by 2 (bps/Hz) to 70-dBm by nearly 4 (bps/Hz).

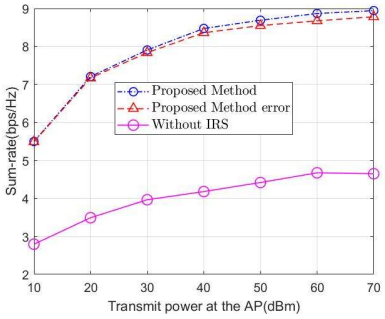

Fig. 3. Comparison of transmission sum rates when the number of users (information receiving end and energy receiving end) is 3, the number of antennas is 16, and the number of reflective elements is 20.

Figure 3 shows the performance comparisons employing 3 users (information receiving end and energy receiving end), 16 antennas and 20 reflective elements with and without RIS. The error part is the 10% parameter error of our proposed method. In addition, whether it is a system with RIS or a system without RIS, the two transmission powers are fixed. It can be seen from the figure that with RIS, the overall rate is faster than that without RIS, from 10-dBm faster than 2 (bps/Hz) to 70-dBm faster than 4 (bps/Hz).

V. Conclusion

In this paper, we study an RIS-assisted SWIPT communication system. Specifically, we want to maximize the transmission sum rate of the system, subject to power constraints and energy harvesting constraints. The transmission sum rate of the system is significantly faster than that of the system without RIS. Some simulation examples are given to demonstrate the effectiveness of the proposed system.

References

[1] L. Lu, G. Y. Li, A. L. Swindlehurst, A. Ashikhmin, and R. Zhang, "An overview of massive MIMO: Benefits and challenges," IEEE J. Sel. Top. Sign. Proces., vol. 8, no. 5, pp. 742 – 758, 2014.

[2] H. Liu, F. Hu, S. Qu et al., "Multipoint wireless information and power transfer to maximize sum-throughput in WBAN with energy harvesting," IEEE Internet Things J., vol. 6, no. 4, pp. 7069 – 7078, 2019.

[3] L. O. Varga, G. Romaniello, Vu ˇ cini´c et al., "Greennet: An energyharvesting IP-enabled wireless sensor network," IEEE Internet Things J., vol. 2, no. 5, pp. 412 – 426, 2015.

[4] G. Yu, X. Chen, C. Zhong et al., "Design, analysis and optimization of a large intelligent reflecting surface aided B5G cellular Internet of Things," IEEE Internet Things J., 2020.

[5] Q. Wu and R. Zhang, "Towards smart and reconfigurable environment: Intelligent reflecting surface aided wireless network," IEEE Commun. Mag., 2019.

[6] ——, "Intelligent reflecting surface enhanced wireless network via joint active and passive beamforming," IEEE Trans. Wireless Commun., vol. 18, no. 11, pp. 5394 – 5409, 2019.

[7] S. Gong, Z. Yang, C. Xing, J. An and L. Hanzo, "Beamforming Optimization for Intelligent Reflecting Surface Aided SWIPT IoT Networks Relying on Discrete Phase Shifts," in IEEE Internet of Things Journal, doi: 10.1109/JIOT.2020.3046929.

[8] S. Zhang and R. Zhang, "Capacity characterization for intelligent reflecting surface aided MIMO communication," IEEE J. Sel. Areas in Commun., 2020.

[9] C. Pan, H. Ren, K. Wang, W. Xu, M. Elkashlan, A. Nallanathan, and L. Hanzo, "Intelligent reflecting surface for multicell MIMO communications," arXiv preprint arXiv:1907.10864, 2019.

[10] Y. Yang, B. Zheng, S. Zhang, and R. Zhang, "Intelligent reflecting surface meets OFDM: Protocol design and rate maximization," IEEE Trans. Commun., 2020.

[11] B. Zheng and R. Zhang, "Intelligent reflecting surface-enhanced OFDM: Channel estimation and reflection optimization," IEEE Wireless Commun. Lett., 2019.

[12] Z. Q. He and X. Yuan, "Cascaded channel estimation for large intelligent metasurface assisted massive MIMO," IEEE Wireless Commun. Lett., 2019.

[13] C. You, B. Zheng, and R. Zhang, "Progressive channel estimation and passive beamforming for intelligent reflecting surface with discrete phase shifts," arXiv preprint arXiv:1912.10646, 2019.

Compound User Scenarios on a Hybrid Cloud

Hui-Shan Chen
National Center for High-performance Computing
National Applied Research Laboratories
Taichung, Taiwan
email: chwhs@narlabs.org.tw

Yi-Lun Pan
National Center for High-performance Computing
National Applied Research Laboratories
Hsinchu, Taiwan
email: serenapan@narlabs.org.tw

***Abstract*—The Information Technology (IT) industry is increasingly adopting hybrid cloud environments, which can leverage the advantages of public and private clouds. The Hybrid Cloud Platform of National Center for High-performance Computing (NCHC) provides flexibility and scalability strategies to meet various cross-cloud scenarios and artificial intelligence applications. Furthermore, based on this cloud architecture, High-Performance Computing (HPC) services are integrated to provide colossal computing power. Therefore, the cloud platform supports various value-added cloud services and applications suitable for various user scenarios.**

Keywords-hybrid cloud; cross-cloud; artificial intelligence; high-performance computing.

I. INTRODUCTION

Based on a highly available, highly reliable, and scalable design, the resource management of NCHC Hybrid Cloud Platform [1] connects with different cloud providers to realize hybrid cloud management of private and public clouds. The cloud platform incorporates multiple cloud technologies, including hyper-converged infrastructure, multi-cloud management tools [2][3], software-defined data centers and private network technology such as Chief Cloud eXchange (CCX) [4]. In Section 2, we introduce the system architecture. Then Section 3, the implementations for user scenarios are described. Finally, we conclude this poster and plan future developments in Section 4.

II. SYSTEM ARCHITECTURE

The NCHC Hybrid Cloud Platform supports diverse cloud services and offers flexible cloud solutions, whether for HPC applications, AI education, disaster recovery, or sensitive application requirements. Figure 1 presents the system architecture of the cloud platform. It leverages cross-cloud resource management to invoke the computing and storage resources of the public cloud for expansion. In order to cope with sensitive needs, the protection of sensitive data and network access control are very important, so the cloud platform also marks out the privacy zone.

The cloud platform is designed to integrate HPC services by designing a Resource Broker [5], an integrated scheduling and management tool for physical and virtualized computing resources. The Resource Broker can leverage various service resources through an API Gateway, including HPC, hybrid cloud, and storage devices.

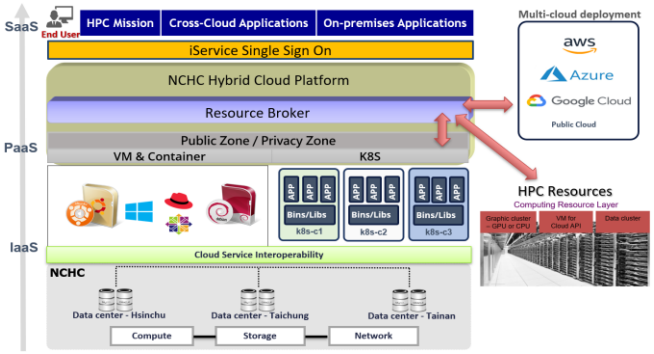

Figure 1. System Architecture

Moreover, Site-to-Site VPNs, private connections, or other network technologies will be established to connect the internal networks of virtual machine service and HPC services. Then, users just need to create a virtual machine as an interactive node to access HPC services. This will enable the cloud platform to perform computational simulations through seamless interaction with HPC resources and public clouds.

III. IMPLEMENTATION FOR USER SCENARIO

Leveraging the elasticity of the public cloud effectively not only achieves system scalability but also significantly reduces costs. The designed scheduling and management tools - Resource Broker can dynamically allocate appropriate computing resources based on demand.

A. *HPC Missions*

When on-premises cloud resources are fully loaded and reach quota limits, users can quickly submit requirements to HPC environments or public clouds to run HPC workloads [6]. We design and develop the integrated functions and interfaces of the cloud platform to bridge the HPC environment and connect HPC resources and storage devices to meet the needs of computing simulations. API Gateway dispatches and triggers all HPC Jobs for execution on computing nodes. The integration shortens researchers' development time and testing cycle, and achieves high-performance benefits.

B. *Cross-Cloud Services*

This research mainly integrates with AWS, so AWS services are used as examples. The Cross-Cloud Services [7] are connected through Site-to-Site VPN or AWS Direct Connect [8].

- **Cloud HPC Service.** The Cloud HPC Parallel Cluster seamlessly integrates on-premises and public cloud resources in hybrid cloud environments. AWS ParallelCluster [9] can automatically deploy and configure the SLURM for automated resource management and job scheduling. Additionally, it can dynamically expand or shrink the number of cloud hosts based on workload and support the job priority mechanism.
- **Disaster Recovery (DR).** An automated disaster recovery framework has been established, and it integrates AWS Elastic Disaster Recovery [10] to offer cloud-based disaster recovery services. Based on a multi-cloud management tool - Morpheus [11], scheduled jobs make it easier to automate system operation and management through workflow. The designed mechanism simplifies the complexity of implementing disaster recovery.
- **Site-to-Site VPN.** To ensure the high availability of cloud services, a secure and reliable private connection provides direct access to the public cloud and on-premises cloud resources when needed. On the hybrid cloud platform, PFSENSE [12] is adopted to replace CCX. Setting up tunnels separately is required for IPsec VPN to provide private networks, as shown in Figure 2. This enables on-premises cloud platforms to take full advantage of the elasticity and scalability provided by public clouds and also reduce costs.

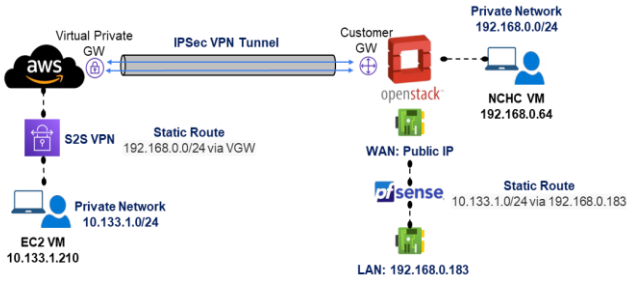

Figure 2. Site-to-Site VPN

C. *On-Premises Applications*

- **AI training and AI Education.** One such application is AI model training for making predictions on new data. Figure 3 shows running AI applications [13] [14] on GPU virtual machines will speed up the model training process and shorten model development time. In addition, it can also be used in the education field to provide teachers with a consistent or customized teaching environment. In this way, it can reduce the cost of IT infrastructure construction and management, and promote the popularization of cloud artificial intelligence education.

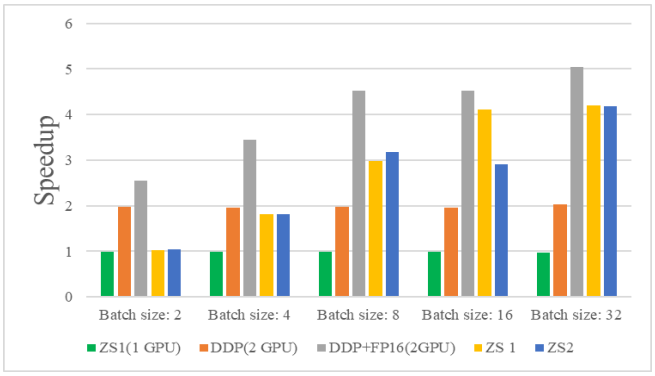

Figure 3. AI Applications

- **Privacy Zone.** This cloud platform provides a private portal, and users need to access and manage resources through a Virtual Desktop Infrastructure (VDI), such as Kasm workspace [15]. Privacy Zone is designed with a fully software-defined architecture to meet privacy requirements. The platform provides adequate network isolation and protection of highly sensitive data. This can ensure that non-approved data remains within the privacy zone, as shown in Figure 4.

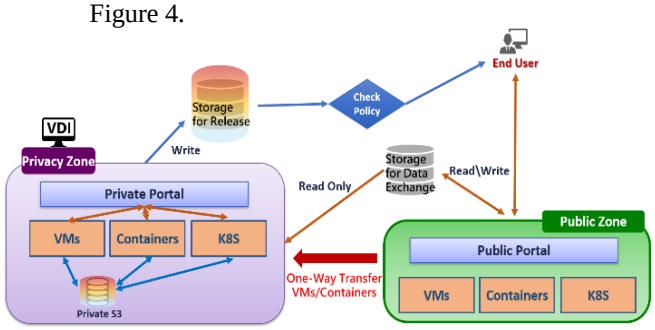

Figure 4. Privacy Zone

Whether it is for the medical field, government agencies, or research centers, information security risks will be significantly improved and avoided in the future.

IV. CONCLUSIONS

When the hybrid cloud platform needs to enlist HPC computing resources, the storage of the privacy zone needs to be synchronized to the computing nodes of the HPC environment. Therefore, our challenges include: (1) Ensuring that sensitive data does not leave the privacy zone. (2) Secure access control when requisitioning HPC resources. (3) Encrypted data transmission. These considerations are crucial for the future development of our platform. It can effectively enhance the security of cross-platform environments and ensure data transmission.

REFERENCES

[1] NCHC Hyper Kylin Hybrid Cloud Platform, URL:https://portal.hci-hybrid.nchc.org.tw/portal, August, 2024.

[2] H. A. Imran et al., "Multi-Cloud: A Comprehensive Review", 2020 IEEE 23rd International Multitopic Conference, Bahawalpur, Pakistan, pp. 1-5, doi: 10.1109/INMIC50486.2020.9318176, 2020.

[3] J. Hong, T. Dreibholz, J. A. Schenkel, and J. A. Hu, "An overview of multi-cloud computing." Web, Artificial Intelligence and Network Applications: Proceedings of the Workshops of the 33rd International Conference on Advanced Information Networking and Applications 33. Springer International Publishing, pp. 1055-1068, 2019.

[4] Chief Telecom Inc, "Chief Cloud eXchange Center[Computer software]", URL:https://en.chief.com.tw/exchange-center/, August, 2024.

[5] P. Subramanian et al., "Progressive Reservation of Cloud Services Using Multi-Cloud Broker System", Engineering Proceedings, 59(1):29, https://doi.org/10.3390/engproc2023059029, 2023.

[6] Q. He, S. Zhou, B. Kobler, D. Duffy, and T. McGlynn, "Case study for running HPC applications in public clouds", In Proceedings of the 19th ACM International Symposium on High Performance Distributed Computing. ACM, pp. 395–401, 2010.

[7] A. Akram, "CRACS: Cross-Cloud Access Control Service for Multi-Cloud SaaS Applications", 2023.

[8] Network-to-Amazon VPC connectivity options, https://docs.aws.amazon.com/whitepapers/latest/aws-vpc-connectivity-options/network-to-amazon-vpc-connectivity-options.html, August, 2024.

[9] T. Dancheva, U. Alonso, and M. Barton, "Cloud benchmarking and performance analysis of an HPC application in Amazon EC2", Cluster Computer, vol. 27, pp. 2273–2290, 2024.

[10] AWS Elastic Disaster Recovery, URL:https://aws.amazon.com/tw/disaster-recovery/, August, 2024.

[11] Patel, G. and S. Patel. "Managing multi-cloud deployment with Morpheus", International Journal of Innovative Technology and Exploring Engineering, vol. 9, no. 3, pp. 1239-1243, 2020.

[12] S. T. Makani, B. P. Panchakarla, and S. R. Pulyala, "Enterprise-Grade Hosted VPN Services with AWS Infrastructure", Journal of Engineering and Applied Sciences Technology, 1-7, 10.47363/JEAST/2022(4)199, 2022.

[13] M. Marei, S. E. Zaatari, and W. Li, "Transfer learning enabled convolutional neural networks for estimating health state of cutting tools", Robotics and Computer-Integrated Manufacturing, Volume 71, 2021.

[14] S. Li et al. "PyTorch Distributed: Experiences on Accelerating Data Parallel Training", 2020.

[15] Kasm Workspaces, URL:https://kasmweb.com/, August, 2024.